IEEE Access
Multidisciplinary | Rapid Review | Open Access Journal

Received December 1, 2019, accepted December 9, 2019, date of publication December 13, 2019,
date of current version December 23, 2019.

Digital Object Identifier 10.1109/ACCESS.2019.2959641

Short-Circuited Stub-Embedded Ring Resonator and its Application in Diplexer

BAOPING REN[1], (Member, IEEE), CHENFEI LE[2], XUEHUI GUAN[1], (Member, IEEE), AND ZHEWANG MA[3], (Member, IEEE)

[1]School of Information Engineering, East China Jiaotong University, Nanchang 330013, China
[2]Information Technology and communication Company, NARI Group Corporation, Nanjing 210000, China
[3]Graduate School of Science and Engineering, Saitama University, Saitama 338-8570, Japan

Corresponding author: Xuehui Guan (xuehuiguan@gmail.com)

This work was supported in part by the National Science Foundation Committee of China, China, under Grant 61761018, Grant 61461020, and Grant 61901170, in part by the Jiangxi Provincial Cultivation Program for Academic and Technical Leaders of Major Subjects, China, under Grant 20162BCB22018, in part by the Natural Science Foundation of Jiangxi Province, China, under Grant 20181BBE58016, Grant 20171BCB24009, and Grant 20192BBE50063, and in part by the Science and Technology 5511 Project of Jiangxi Province, China, under Grant 20165BCB19010.

ABSTRACT Two types of short-circuited stub-embedded ring resonators (SERRs) are proposed in this paper. The resonant modes of the SERR can be designed by properly choosing the short-circuited point on the resonator. When the short-circuited point is set at the open-end of embedded-stub, type A resonator is realized and large frequency ratio of harmonic to fundamental frequency can be achieved. Simultaneously, wide stopband can be realized. When the short-circuited point is set at the loop portion of SERR, type B resonator is realized and low frequency ratio of harmonic to fundamental frequency can be achieved. These characteristics of the resonators type A and type B are explored and combined in a diplexer with common resonator part. Each channel of the diplexer are constructed by using the type A resonators for wide stopband, and then combined via a type B resonator for designated frequencies. A third-order diplexer operating at 3.45/5.8 GHz for fifth generation of mobile communications (5G) and wireless local area networks (WLAN) is designed, fabricated, and measured. Measured results agree well with the simulated ones, which confirms the proposed design methodology.

INDEX TERMS Common resonator, diplexer, short-circuited stub-embedded ring resonator (SERR), wide stopband.

I. INTRODUCTION

As a essential component of RF front end, the diplexer has been widely applied in modern high quality wireless communication systems, including CDMA, WLAN and LTE [1]–[4]. The most common approach to realize a diplexer is to combine two bandpass filters (BPFs) through an impedance- matching junction with two branches [5]–[8]. In [5], a diplexer is constructed by connecting two BPFs via a Y-junction to achieve high selectivity. In [6], compact hybrid resonators are used to design a miniaturized diplexer through a T-junction. High stopband rejection and output isolation can be realized by properly allocating the controllable transmission zeros of filters at the desired frequencies. In [7], the diplexer with two transmission zeros in each channel is formed by connecting two dual-mode resonators through a bent T-junction. Based on the fact that a diplexer usually consists of two BPFs with different central frequencies, the simplest means for miniaturization of a diplexer is to reduce the sizes of each filter. To achieve this goals, several types of diplexers have been proposed using planar resonators such as the U-shaped hairpin line resonator [9], the open loop resonators [10], and the hybrid resonators [11]. Total size of the diplexers are dramatically reduced by applying novel compact resonators. However, the size is unexpectedly large due to the existence of matching junction, especially at the lower frequency band. In this aspect, some diplexers are designed by combining two filters through common resonator sections. In [12], the fundamental and the first spurious resonant frequency of stepped-impedance resonator (SIR) are shared by both channel filters of a diplexer. In [13], a T-shaped structure, which works as a common resonator, is introduced

The associate editor coordinating the review of this manuscript and approving it for publication was Andrei Muller.

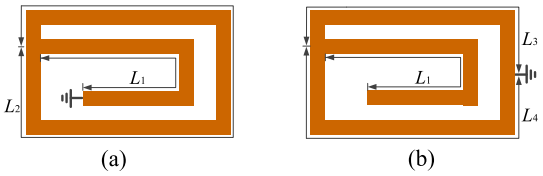

FIGURE 1. Short-circuited stub-embedded ring resonator. (a) Type A, and (b) Type B.

to replace the conventional matching network, resulting in significant size reduction of the constituted diplexer. In [14], two dual-resonance spiral resonators are used as common resonator to ensure compact size of diplexer. Furthermore, in order to improve IP3 performance of the circuit, diplexer with high suppression level in stopband (frequency ratio of the spurious to the lower channel of the diplexer) is preferred. In [15], three different SIRs with the same fundamental frequency and different spurious frequencies are applied in the diplexer to extend the stopband. In [16] and [17], the wide stopband characteristics are achieved by using short-circuited microstrip resonators. To our best knowledge, it is still a challenging work to develop diplexer with compact size and wide stopband.

In this paper, a compact microstrip diplexer with wide-stopband is presented. The diplexer is composed of two types of short-circuited stub-embedded ring resonators (SERRs). Resonant characteristics of the proposed SERRs with different short-circuited positions are studied and compared. The relationship between electrical lengths and resonant properties of short-circuited SERR is discussed in detail. Based on the analysis of the resonator, their resonant modes can be easily allocated and tuned for versatile applications. To verify this methodology, a third-order diplexer operating at 3.45/5.8 GHz is designed using two types of short-circuited SERR. Finally, the proposed diplexer is fabricated and measured. The measurements match the simulations well and reveal the device's high performance.

II. CHARACTERISTICS OF SHORT- CIRCUITED SERR

Circuit diagram of the proposed two short-circuited SERR are presented in Fig. 1. The proposed resonator is constructed by using a uniform impedance ring resonator and a stub. The stub is embedded in the ring resonator to get a compact size. Two short-circuited positions are chosen for different resonant characteristics. As shown in Fig. 1(a), the short-circuited portion is applied on the end point of the stub, where type A resonator can be achieved. On the other hand, when the short-circuited portion is applied on the ring portion, type B resonator is realized, as depicted in Fig. 1(b). L_1 and L_2 denote the physical lengths of the stub and the ring, respectively. L_3 and L_4 indicate the physical lengths of the upper and lower segments from tap-point to the short-circuited point, respectively.

Equivalent circuit of type A resonator is given in Fig. 2(a). The corresponding electrical lengths and characteristic admittance are referred to θ_1, θ_2, θ_3, θ_4, θ_5 and Y_1, Y_2, Y_3,

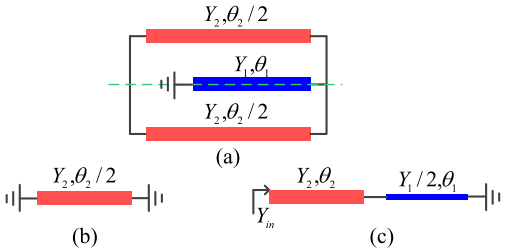

FIGURE 2. Equivalent circuit of type A resonator. (a) Original circuit, (b) Odd-mode, and (c) Even-mode.

Y_4, Y_5, respectively. Herein, $\theta_1 = \beta L_1$, $\theta_2 = \beta L_2$, $\theta_3 = \beta L_3$, $\theta_4 = \beta L_4$, and $\theta_5 = \beta L_5$, where β is the propagation constant. Its odd-mode and even-mode equivalent circuits are presented in Fig. 2(b) and 2(c), respectively. When the circuit is excited by odd-modes, the symmetrical plane works as electric wall and it can be seen as short circuited point, which leads to the equivalent circuit shown in Fig. 2(b), and its resonant condition can be derived as

$$\tan(\theta_2/2) = 0 \tag{1}$$

When the circuit is excited by even-modes, the symmetrical plane works as magnetic wall and it can be seen as open circuited point, which leads to the equivalent circuit shown in Fig. 2(c). Ignoring the discontinuity of stepped impedance, its resonant condition can are expressed by

$$Y_1 \cot\theta_1 - 2Y_2 \tan(\theta_2/2) = 0 \tag{2}$$

To have a clearer knowledge of the resonant characteristics of the resonator, frequency ratio (r) net-type graph of the type A resonator with varied admittance ratio $K(K = Y_1/Y_2)$ and stub length α ($\alpha = 0.5\theta_2/(\theta_1 + 0.5\theta_2)$) is plotted in Fig. 3. As shown in Fig. 3(a), the smaller admittance ratio is, the lager frequency ratio can be achieved under even-mode excitation. The r has the maximum value ($K < 1$) and the minimum value ($K > 1$) when α is approximately 0.5. When K equals 1, it can be seen as a short circuited uniform impedance resonator, and the r is always 3. As shown in Fig. 3(b), the smaller electric length ratio is, the lager frequency ratio can be achieved under odd-mode excitation. From Fig. 3, it can be concluded that the type A resonator can realize a wider degree control of frequency ratio of harmonic to fundamental frequency by changing K. Therefore, wide stopband performance can be realized.

The equivalent circuit of proposed type B resonator that short-circuited at ring edge is presented in Fig. 4(a). Electrical lengths of the loaded stub, upper and lower portion of ring resonator are θ_3, θ_4, and θ_5, respectively. For analysis simplification, herein $Y_3 = Y_4 = Y_5 = Y$ is assumed. As shown in Fig. 4(b), Y_{in1} and Y_{in2} represent the corresponding input admittance from the up and down sides of the stub-loaded node, respectively. Its resonant condition can be derived as

$$\mathrm{Im}(Y_{in1} + Y_{in2}) = 0 \tag{3}$$

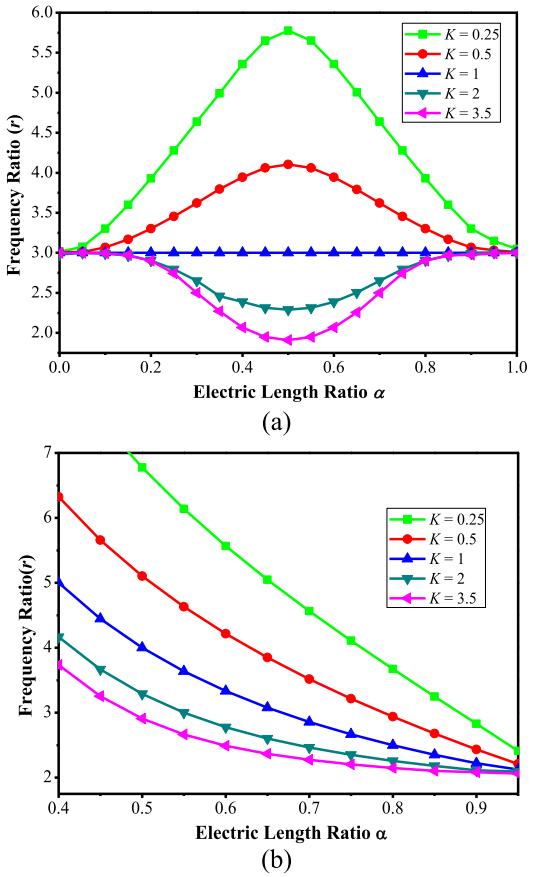

FIGURE 3. (a) Normalized even-mode resonant frequencies versus K and α. (b) Normalized odd-mode resonant frequencies versus K and α.

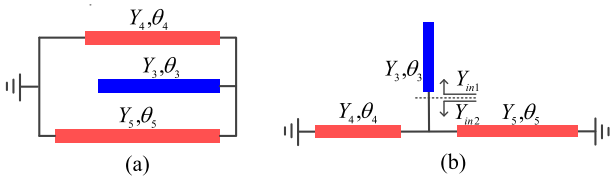

FIGURE 4. Equivalent circuit of type B resonator. (a) Original circuit and (b) Simplified circuit.

where

$$Y_{in1} = jY \tan\theta_3 \tag{4}$$

$$Y_{in2} = -j\left(Y \cot\theta_4 + Y \cot\theta_5\right) \tag{5}$$

Substituting (4) and (5) into (3), the resonant condition for proposed resonator that shorted at ring edge can then be expressed as

$$\tan\theta_3 - \cot\theta_4 - \cot\theta_5 = 0 \tag{6}$$

Therefore, the resonant frequencies can be ascertained from the root of (6). Herein, $\theta_3 + \theta_4 = 90°$ is assumed for simplification. Thus, (6) can be rewritten as

$$\tan\left(r_i\theta_3\right) - \cot\left[r_i\left(90° - \theta_3\right)\right] - \cot\left(r_i\theta_5\right) = 0 \tag{7}$$

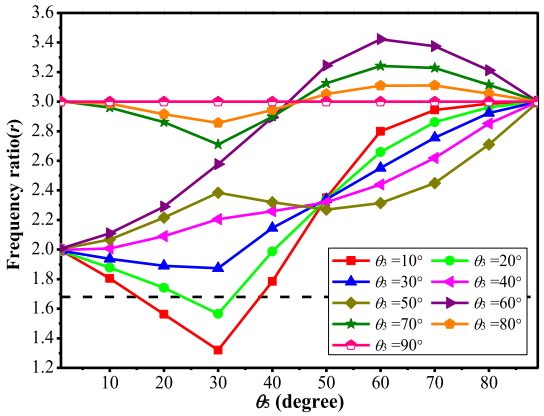

FIGURE 5. Resonant design graphs for the type B resonator with varied stub lengths θ_3 and θ_5.

where $r_i = f_i/f_0$ $(i = 1, 2)$ is the normalized fundamental frequency of one half-wavelength resonator with electrical length $2(\theta_3 + \theta_4)$. Once θ_3 and θ_5 are determined, there exist two solutions of r_i at the finite scope by solving (7). Based on the above discussion, frequency ratio $r(r_2/r_1)$ net-type graph of the type B resonator is finally plotted in Fig. 5. It can be seen that frequency ratio increases as θ_3 changes from 10° to 90° when θ_5 is fixed in the range of 1° to 45°. In the range from 45° to 90° of θ_5, the frequency ratio r decreases as θ_3 changes from 60° to 90°, and 10° to 50°. The frequency ratio is fixed at 3 when θ_5 is approximated 0° and θ_5 is chosen range of 70° to 90°, but it is fixed at 2 when θ_5 is approximated 0° and θ_5 is chosen range of 10° to 60°. This phenomenon is attribute to that the resonant modes of former situation are mainly produced by short-circuited quarter- wavelength portion of type B resonator, while resonant modes of later situation are mainly produced by half-wavelength portion. From Fig. 5, it can be observed that the type B resonator can realize wider degree control of frequency ratio of harmonic to fundamental frequency. Transmission coefficient S_{21} for different L_1, L_3 and L_4 of type B resonator under weak coupling are plotted in Fig. 6. It can be seen that resonant frequency ratio increases as L_1 increases or L_3 decreases, where L_4 is fixed. Furthermore, when L_1 and L_3 are fixed, frequency ratio increases as L_4 increases. Simulated results of the resonator agree well with the ideal prediction.

For proposed two types of short-circuited SERR in Figure 1, the physical dimension of resonators can be chosen as an arbitrary value so that more design freedoms will be obtained. For design simplicity, $Y_1 = Y_2 = Y_3 = Y_4 = Y_5$ is assumed in this paper. The mode-splitting characteristics of short-circuited SERR that shorted at ring edge can be controlled by the electrical length parameters of the resonator.

III. DESIGN OF MICROSTRIP DIPLEXER

To confirm the validity and flexibility of this new resonator, a diplexer operated at 3.45/5.8 GHz for potential applications in 5G and WLAN is presented. The diplexer is constructed by using a common resonator structure. Since the frequency

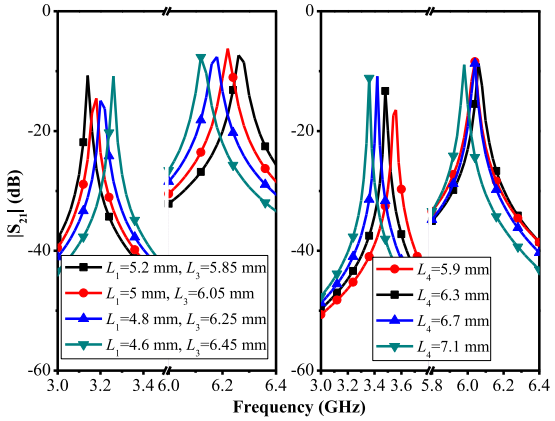

FIGURE 6. Frequency response of S_{21} for different L_1, L_3 and L_4 of type B resonator under weak coupling.

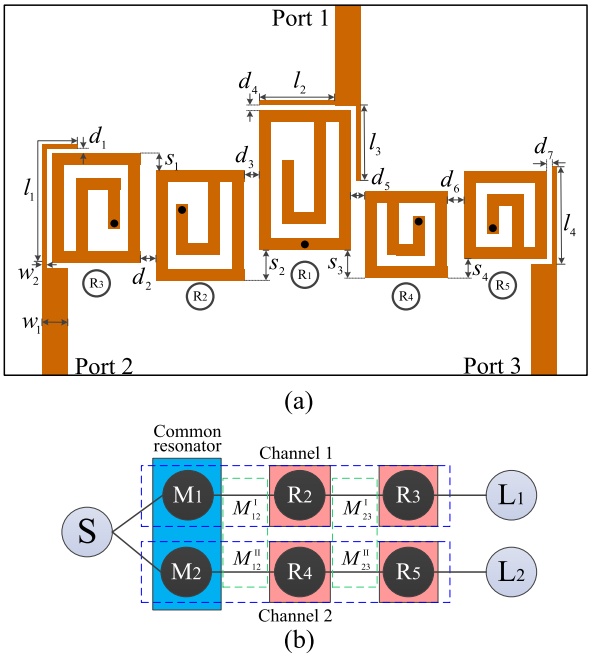

FIGURE 7. (a) Layout of the designed diplexer, and (b) coupling scheme of the proposed diplexer.

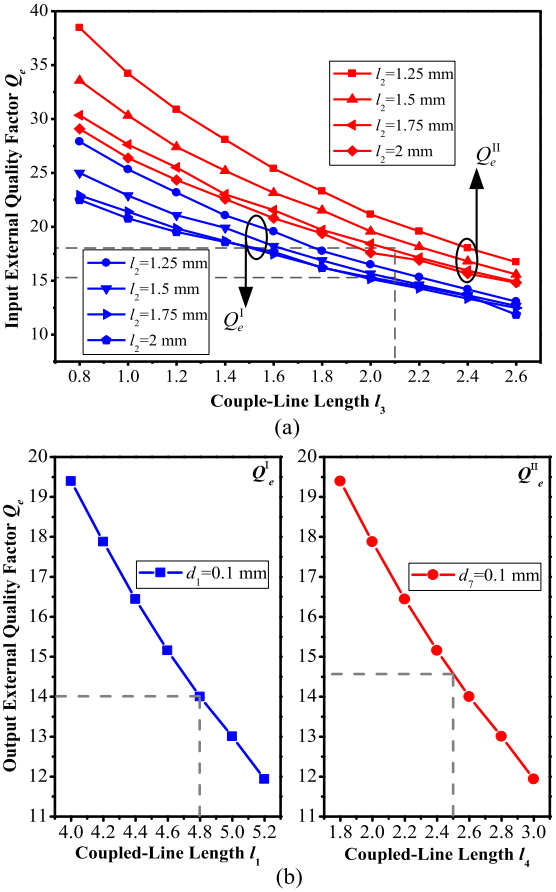

FIGURE 8. (a) Input Q_e versus the coupled-line length l_3 when $d_4 = 0.05$ mm. (b) Output Q_e versus the coupled-line length l_1 and l_4 when $d_1 = 0.1$ mm and $d_7 = 0.1$ mm.

ratio of higher channel to lower channel is less than 2, type B resonator is chosen for the common resonator, and type A resonator is chosen for individual channels, as shown in Fig. 7. For the type B resonator, as revealed in Fig. 5, two modes of the proposed resonator can be quickly determined according to the desired frequencies of channels by properly choosing the values of θ_3 and θ_5. In this design, f_0 is chosen 2.2 GHz for normalization. Thus, two resonant frequencies, denoted as f_1 and f_2 of the designed resonator will be finally obtained. The normalized resonant frequency ratio in this design is computed as follows: $f_2/f_1 = 5.8/3.45 \approx 1.68$. A series of suitable points (dash red line in Figure 5) for realizing the target frequency ratio can be quickly found in Fig. 5. The corresponding θ_3, θ_4, and θ_5 are then found to be 25, 65, and 30, respectively. As to type A resonator, $K = 1$ and $\alpha = 0.6$ are chosen from Fig. 3, and a wide-stopband characteristic can be obtained.

Based on the proposed two-type SERRs that short-circuited portion are allocated at end point of embedded stub and the ring edge, a diplexer with third-order Chebyshev response and equal ripple of 0.043dB in each channel is designed. Fig. 7(a) depicts the layout of the diplexer designed on a 0.8 mm-thick substrate with a relative dielectric constant of 10.2 and loss tangent of 0.0023. Two resonant modes of R_1 are used in diplexer, and only one mode of other resonators is utilized in this design. On one hand, R_1, R_2, and R_3 form the low-frequency channel. Gaps d_2 and d_3 provide the inter-resonator electric coupling, which can be controlled by the gap width (d_3 and d_2) and the staggered distance (s_2 and s_1). The external output coupling adopts the high impedance microstrip line and its length (l_1) and coupling gap (d_1) determine the coupling strength. On the other hand, R_1, R_4, and R_5 form the high-frequency channel. Gap d_5 and d_6 provide the inter-resonator electric coupling, whose strength can be controlled by the gap width (d_5 and d_6) and the staggered distance (s_3 and s_4). The high impedance microstrip length (l_4), width (w_2), and coupling gap (d_7) determine the output coupling strength. The length of coupling line (l_2, l_3)

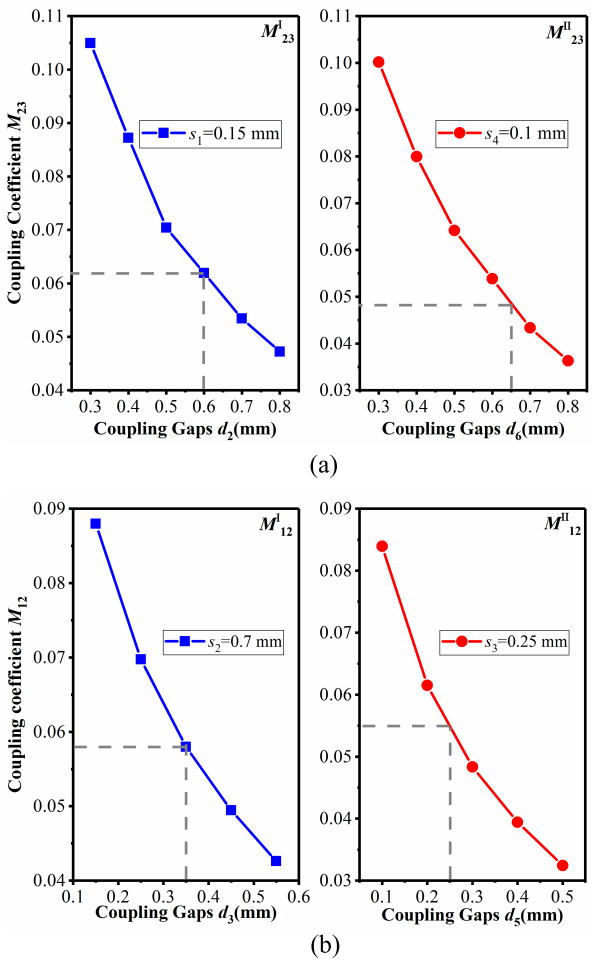

FIGURE 9. (a) M_{12} of two channels under different coupling gaps. (b) Coupling coefficients M_{23} of two channels under different coupling gaps.

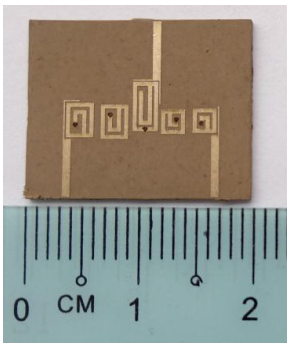

FIGURE 10. Photograph of the fabricated microstrip diplexer.

and width of coupling gap (d_4) determine the input coupling strength of two channels because that common resonator is utilized in this design. Figure 7(b) shows the coupling scheme of the proposed diplexer. Incident signal at source is split into two ways via the common resonator R_1. Two resonant modes of R_1, i.e., M_1 and M_2, are used for the lower channel 1 at 3.45 GHz and the upper channel 2 at 5.8GHz, respectively. M1 is coupled to resonators R_2 and R_3, and then to output port L_1 in upper side of Fig. 7(b). Similarly, M_2 is coupled

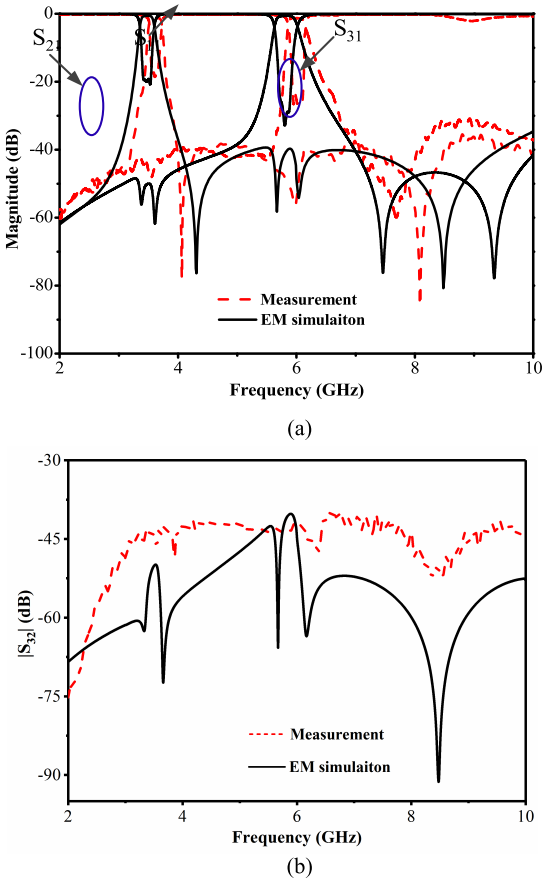

FIGURE 11. Simulated and measured frequency responses of the proposed diplexer. (a) S_{11}, S_{21}, and S_{31} (b) S_{23}.

TABLE 1. Geometrical dimensions of the microstrip.

Parameter	w_1	w_2	d_1	d_2	d_3	d_4
Value (mm)	0.75	0.15	0.1	0.6	0.35	0.05
Parameter	d_5	d_6	d_7	s_1	s_2	s_3
Value (mm)	0.25	0.65	0.1	0.15	0.7	0.25
Parameter	s_4	l_1	l_2	l_3	l_4	
Value (mm)	0.1	4.6	1.75	2.15	2.55	

to resonators R_4 and R_5, and then to the output port L_2 in lower-side of Fig. 7(b).

The center frequencies and fractional bandwidths (FBWs) of the diplexer are $f_{c1} = 3.45$ GHz, $f_{c2} = 5.8$ GHz and $\Delta_{c1} = 4.3\%$, $\Delta_{c2} = 3.6\%$, where the subscripts c1 and c2 denote the first and second channels, respectively.

The proposed diplexer can be equivalent to the design of two similar resonator-coupled BPFs, where each channels can be designed individually [18]. The lumped circuit element values of the low-pass prototype filter are found to be $g_0 = 1$, $g_1 = 0.8516$, $g_2 = 1.1032$, $g_3 = 0.8516$, and $g_4 = 1$. The coupling coefficients and the external quality

factors can be deduced as $M^{I12} = 0.046$, $M^{I23} = 0.046$, and $Q^{Ie} = 16.4$ for the 3.45 GHz channel, $M^{II12} = 0.039$, $M^{II23} = 0.039$, and $Q^{IIe} = 19.6$ for the 5.8 GHz channel [19]. The EM simulator *Sonnet* is used to extract the desired parameters for two channels.

Figure 8 plots the extracted design curves of external Q_e of input port and output port for proposed diplexer. The width of the high-impedance microstrip line, w_2, is set to 0.15 mm. In order to satisfy the required Q_e of both channels simultaneously, the coupled length $l_2 = 1.75$ mm and $l_3 = 2.15$ mm are chosen from Fig. 8(a), thus $l_1 = 4.8$ mm and $l_4 = 2.5$ mm are chosen from Fig. 8(b).

Figure 9(a) depicts coupling coefficient M_{12} versus with the coupling gap d_3 and d_5 on the condition of $s_2 = 0.7$ mm and $s_3 = 0.25$ mm. Figure 9(b) depicts the characteristics of the M_{23} with different coupling gaps(d_2 and d_6). In order to satisfy the coupling coefficients for both channels simultaneously, the coupled length $d_3 = 0.35$ mm and $d_5 = 0.25$ mm are chosen from Figure 9a, as well as $d_2 = 0.6$ mm and $d_6 = 0.65$ mm are chosen from Fig. 9(b). Following the above-mentioned design steps, the geometrical dimensions of the proposed common resonator are chosen as follows: $L_1 = 6.2$ mm, $L_3 = 7.15$ mm, $L_4 = 5.6$ mm from Fig. 1(b), and the low and high channel resonator are chosen 3.35 mm, 9.6 mm and 1.75 mm, 7.1 mm as L_1 and L_2 from Fig. 1(a), respectively, and the diameter of short-circuited via is chosen 0.3 mm. The geometrical dimensions are listed in Table 1.

IV. IMPLEMENTATION OF MICROSTRIP DIPLEXER

For demonstration purposes, the designed diplexer is fabricated on the TP-2 substrate with a relative dielectric constant of 10.2, loss tangent of 0.0023, and thickness of 0.8 mm. Fig. 10 shows a photograph of the fabricated diplexer. The size of the entire diplexer is 14 mm × 5.2 mm, which amounts to 0.42 $\lambda_g \times$ 0.157 λ_g (λ_g is the guided wavelength of the 50 Ω line on the substrate at the central frequency of the lower band).

Figure 11 shows a comparison between the simulated and measured results of the diplexer, where simulated and measured results are denoted by solid and dashed lines, respectively. The curve shapes of simulated and measured results are in good agreements except a frequency shift. The small frequency shift is mainly caused by the deviation of the dielectric constant of substrate with its nominal value. Upon the above mentioned reason, the the frequency shift of transmission zero is mainly caused by the fabricated error, particularly the error from short-circuiting technique. The simulated results reveals that the diplexer exhibits two channels with central frequencies of 3.45 and 5.8 GHz, and the fractional bandwidths are about 4.06 % and 3.62 %, respectively. The simulated results clearly demonstrate the emergence of three transmission poles in each channel. The measured insertion losses in two channels are found to be 1.2 and 1.3 dB, inclusive of transition loss from the SMA connectors. The simulated and the measured isolation between Port 2 and Port 3 are higher than 40 dB. It is obvious that the out-of-band rejections of the proposed diplexer are better than 30 dB up to 3 f_{c1} (f_{c1} is the lower channel center frequency of the diplexer) over the measured frequency range, result in good stopband responses.

TABLE 2. Comparison between proposed diplexer with referenced ones.

Ref.No	Isolation (dB)	Circuit size ($\lambda_g \times \lambda_g$)	1st/2nd Passbands IL (dB)	Stopband suppression level (dB)
[7]	>33	0.35×0.19	1.76/2.48	30 up to 2.4f_1
[8]	>43	0.79×0.2	1.65/2.25	NA
[9]	>40	0.29×0.29	0.4/0.5	NA
[11]	>55	0.48×0.75	0.94/1.04	NA
[12]	>30	0.71×1.56	2.8/3.2	NA
[13]	>35	0.36×0.38	1.2/1.5	NA
[14]	>39	0.12×0.073	0.41/0.41	30 up to 3.3f_1
[16]	>30	0.58×0.54	NA	30 up to 3.6f_1
[17]	>30	0.2×0.34	2.2/2.1	30 up to 2.8f_1
This work	**>40**	**0.42×0.157**	**1.2/1.3**	**30 up to 3.0f_1**

A comparison about the isolation, circuit size, insertion loss (IL), and stopband suppression level between the proposed diplexer and other referenced ones is listed in Table 2. It can be observed that the proposed diplexer shows the advantages of compact size and wide-stopband. Furthermore, the high isolation of proposed diplexer has been achieved. The designed diplexer is suitable for 5G and WLAN applications and designed resonator can be applied in high performance filters and diplexers.

V. CONCLUSION

A compact and wide-stopband microstrip diplexer with a common resonator has been presented in this paper. The diplexer is mainly composed of two types of short-circuited SERR. The design graphs of the relationship between resonator parameters of electrical length and resonance performances are exploited. To verify this methodology, a third-order dual-channel diplexer operating at 3.45/5.8 GHz is designed, fabricated, and measured. The designed diplexer with compact size and wide stopband. A satisfactory agreement between the measurements and simulations has verify the validity of the proposed principle.

REFERENCES

[1] Z. Li, X. Tang, D. Lu, Z. Cai, Y. Liu, and J. Luo, "Low-loss wide-tuning-range three-pole frequency-agile bandpass diplexer with identical constant absolute bandwidth," *IEEE Access*, vol. 7, pp. 149833–149835, 2019.

[2] K. Song, Y. Zhou, Y. Chen, A. M. Iman, S. R. Patience, and Y. Fan, "High-isolation diplexer with high frequency selectivity using substrate integrate waveguide dual-mode resonator," *IEEE Access*, vol. 7, pp. 116276–116683, 2019.
[3] X. Guo, L. Zhu, and W. Wu, "Balanced Diplexers based on inner-coupled dual-mode structures with intrinsic common-mode suppression," *IEEE Access*, vol. 5, pp. 26774–26782, Dec. 2017.
[4] M. Weng, Y. Hun, and Y. Su, "A hairpin line diplexer for direct sequence ultra-wideband wireless communications," *IEEE Microw. Wireless Compon. Lett.*, vol. 17, no. 7, pp. 519–521, Jul. 2007.
[5] V. K. Velidi, U. Prabhakaran, A. V. G. Subramanyam, D. Sivareddy, and V. V. Srinivasan, "Design of compact microstrip diplexer with high selectivity," in *Proc. Int. Conf. Signal Process. Commun.*, Bengaluru, India, Jul. 2012, pp. 1–4.
[6] T. Yang, P.-L. Chi, and T. Itoh, "High isolation and compact diplexer using the hybrid resonators," *IEEE Microw. Wireless Compon. Lett.*, vol. 20, no. 10, pp. 551–553, Oct. 2010.
[7] Q. Duan, K. Song, F. Chen, and Y. Fan, "Compact wide-stopband diplexer using dual mode resonators," *Electron. Lett.*, vol. 51, no. 14, pp. 1085–1087, Jul. 2015.
[8] C. Zhu, L. Yao, and J. Zhou, "Novel microstrip diplexer based on a dual-band bandpass filter for WLAN system," in *Proc. Asia–Pacific Microw. Conf.*, Yokohama, Japan, Dec. 2010, pp. 1102–1105.
[9] Q. Zhang, Y. Bian, J. Guo, B. Cui, J. Wang, T. Yu, L. Gao, Y. Wang, C. Li, X. Zhang, H. Li, C. Gao, and Y. He, "A compact HTS duplexer for communication application," *IEEE Trans. Appl. Supercond.*, vol. 20, no. 1, pp. 2–7, Feb. 2010.
[10] J. Konpang, "A compact diplexer using square open loop with stepped impedance resonators," in *IEEE Radio Wireless Symp. Dig.*, Orlando, FL, USA, Jan. 2009, pp. 91–94.
[11] S. Srisathit, S. Patisang, R. Phromloungsri, S. Bunnjaweht, S. Kosulvit, and M. Chongcheawchamnan, "High isolation and compact size microstrip hairpin diplexer," *IEEE Microw. Wireless compon. Lett.*, vol. 20, no. 10, pp. 551–553, Oct. 2010.
[12] C.-F. Chen, T.-Y. Huang, C.-P. Chou, and R.-B. Wu, "Microstrip diplexers design with common resonator sections for compact size, but high isolation," *IEEE Trans. Microw. Theory Techn.*, vol. 54, no. 5, pp. 1945–1952, May 2006.
[13] X. Guan, F. Yang, H. Liu, and L. Zhu, "Compact and high-isolation diplexer using dual-mode stub-loaded resonators," *IEEE Microw. Wireless compon. Lett.*, vol. 24, no. 6, pp. 1945–1952, Jun. 2014.
[14] X. Guan, F. Yang, H. Liu, Z. Ma, B. Ren, W. Huang, and P. Wen, "Compact, low insertion-loss, and wide stopband HTS diplexer using novel coupling diagram and dissimilar spiral resonators," *IEEE Trans. Microw. Theory Techn.*, vol. 64, no. 8, pp. 2581–2859, Aug. 2016.
[15] S. Tantiviwat, N. Intarawiset, and R. Jeenawong, "Wide-stopband, compact microstrip diplexer with common resonator using stepped-impedance resonators," in *Proc. IEEE Tencon-Spring*, Sydney, NSW, Australia, Apr. 2013, pp. 174–177.
[16] W. Feng, X. Gao, and W. Che, "Microstrip diplexer for GSM and WLAN bands using common shorted stubs," *Electron. Lett.*, vol. 50, no. 20, pp. 1486–1488, Sep. 2014.
[17] J. Yan, H. Zhou, and L. Cao, "Compact diplexer using microstrip half- and quarter-wavelength resonators," *Electron. Lett.*, vol. 52, no. 19, pp. 1613–1615, Oct. 2016.
[18] L. Bo, Y. Hao, and M. J. Lancaster, "Synthesis of coupling matrix for diplexers based on a self-adaptive differential evolution algorithm," *IEEE Trans. Microw. Theory Techn.*, vol. 58, no. 8, pp. 1945–1952, May 2018.
[19] J. S. Hong and M. J. Lancaster, *Microwave Filter for RF/Microwave Application*. New York, NY, USA: Wiley, 2001.

BAOPING REN (S'16–M'19) received the B.S. degree in communication engineering and the M.S. degree in communication and information system from East China Jiaotong University, Nanchang, China, in 2011 and 2014, respectively, and the Ph.D. degree in microwave engineering from Saitama University, Saitama, Japan, in 2019.

From July 2014 to March 2019, he was with the Jiangxi RF Communications and Sensor Networks Key Laboratory, East China Jiaotong University, as a Research Associate, where he is currently an Assistant Professor. His current research interests include microwave circuits and devices and high-temperature superconducting filters.

CHENFEI LE received the B.S. degree in electronic information science and technology from the Jiangxi University of Science and Technology, Ganzhou, China, in 2015, and the M.S. degree in information and communication engineering from the Jiangxi RF Communications and Sensor Networks Key Laboratory, East China Jiaotong University, Nanchang, China, in 2019.

He joined NARI Information & Communication Technology Company, Ltd., as an Assistant Engineer. His current research interests include microwave circuits and devices and high-temperature superconducting filters.

XUEHUI GUAN (M'11) received the B.S. degree in communication engineering from Jiangxi Normal University, Nanchang, China, in 1988, and the Ph.D. degree in electromagnetic fields and microwave techniques from Shanghai University, Shanghai, China, in 2007.

In 2012, he was a Senior Researcher Associate with the School of Electrical and Electronic Engineering, City University of Hong Kong, Hong Kong. Since June 2013, he has been a Visiting Scholar with the School of Electrical and Electronic Engineering, Nanyang Technological University, Singapore. In 2016, he became a Professor with East China Jiaotong University, Nanchang. His current research interests include radio frequency and microwave passive circuits and systems, synthesis theory and realization of microwave filters, and antennas for wireless communications.

ZHEWANG MA (M'96) received the B.Eng. and M.Eng. degrees from the University of Science and Technology of China (USTC), Hefei, China, in 1986 and 1989, respectively, and the Dr.Eng. degree from the University of Electro-Communications, Tokyo, Japan, in 1995.

In 1996, he was a Research Assistant with the Department of Electronic Engineering, University of Electro-Communications, in 1997, and became an Associate Professor. From 1998 to 2008, he was an Associate Professor with the Department of Electrical and Electronic Systems, Saitama University, where he became a Professor, in 2009. His current researches are mainly concerned with the development of microwave and millimeter-wave devices and circuits, measurements of dielectric materials, and high-temperature superconductors.

Dr. Ma is a member of the Review Board of the *IEICE Transactions on Electronics*. He is a Senior Member of the Institute of Electronics, Information and Communication Engineers (IEICE), Japan. He was a member of the Steering and/or Technical Committees of the 2002, 2006, and 2010, Asia–Pacific Microwave Conference. From 1994 to 1996, he was a Research Fellow of the Japan Society for the Promotion of Science (JSPS). He was a recipient of the Japanese Government Graduate Scholarship, from 1991 to 1993. He was also a recipient of the URSI Young Scientist Award, in 1993. He is the Vice-President of the Technical Group on Electronics Simulation Technology, Electronics Society, IEICE. He has served on the Editorial Board of the IEEE TRANSACTIONS ON MICROWAVE THEORY AND TECHNIQUES and the Review Board of the IEEE MICROWAVE AND WIRELESS COMPONENTS LETTERS.